



# Theoretical study of electronic structure and absorption spectra of diacid and zinc species of series of *meso*-phenylporphyrins

Ying-Hui Zhang\*, Li-Hong Zhao, Wen-Juan Ruan, Yao Xu

Department of Chemistry, Nankai University, 94 Weijin Road, Tianjin 300071, China

## ARTICLE INFO

### Article history:

Received 18 January 2011

Received in revised form 26 April 2011

Accepted 29 April 2011

### Keywords:

*meso*-Phenylporphyrins

Electronic structure

Absorption spectra

Redshift

## ABSTRACT

DFT and TDDFT calculations with density functionals (PBE1PBE, B3LYP, and PBEPBE) have been employed in a study of HCl-acidified diacids of a series of *meso*-phenylporphyrins. This study aims to clarify the influence of conformational distortion, *meso*-phenyl substituents, and counterion Cl<sup>-</sup> on absorption spectra of porphyrin derivatives. Calculations indicate that all three factors increase the MO's level and decrease the Gouterman HOMO–LUMO gap; this, further, brings about the redshift of absorption band. In comparison with experimental methods, the PBE1PBE method produces a more credible description of UV–vis spectra than other two methods. TDDFT calculation with the PBE1PBE method indicates that the electronic effect of the *meso*-phenyl group is dominant for the spectral redshift of porphyrin diacid series as observed in zinc porphyrins. The redshift of the B band of porphyrin diacids is primarily caused by an electron-donating effect of the *meso*-phenyl group, whereas the Q band is more sensitive to the  $\pi$  electron delocalization effect. The counterion is indispensable in a theoretical study of electronic and spectral structure of porphyrin diacids.

© 2011 Elsevier B.V. All rights reserved.

## 1. Introduction

Several spectroscopic methods have proved that peripheral substitution has a significant influence on electronic and spectral features of porphyrins [1–5]. A good understanding of structure–spectra relationship is very important in the design of novel artificial materials. Absorption spectroscopy has been used widely in the study of structural variation in porphyrin rings. As a general phenomenon, the spectral shift has attracted much attention and has been ascribed to the change of electronic structure induced by several factors, such as the electronic effect of substituent, out-of-plane distortion, and the change of bond length and bond angle—called in-plane nuclear reorganization (IPNR) by DiMaggio and co-workers [6,7]. The combined action of several factors, frequently, confounds the identification of the primary cause of spectral shift; therefore, this has given rise to certain debates in the past decades [6–10].

Porphyrin diacids, as an important derivative, have attracted much attention in the past decades because of their marked out-of-plane distortion and novel spectral features with regard to neutral porphyrin [11–15]. Studies on the electronic structure and spectral variation of porphyrin diacids have been carried out by certain groups of researchers [16–19]. Although providing certain impor-

tant insights, these studies focus only on a single aspect and, therefore, lack comprehensive and systematic understanding of the spectral features of porphyrin diacids.

In this article, we present a theoretical analysis of the influence of several typical factors (including conformational distortion, *meso*-phenyl substituent, and counterion Cl<sup>-</sup>), on electronic structure and absorption spectra of a series of *meso*-phenylporphyrin diacids (structure depicted in Fig. 1). Zinc complexes were also studied because their 4-fold symmetry and near-planar geometry were expected to generate beneficial information. Meanwhile, PBE1PBE, B3LYP, and PBEPBE methods were compared, particularly in spectra simulation. Comparison with experimental methods indicates that the PBE1PBE method produces a more credible description of absorption structure, particularly for the Q band, of porphyrin diacids than the B3LYP and PBEPBE methods. Further, analysis indicates that the electronic effect of the *meso*-phenyl group is the main cause for the absorption redshift of porphyrin diacids series with increased *meso*-phenyl substitution.

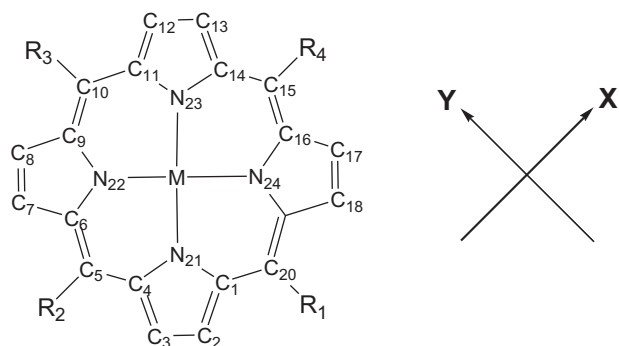
## 2. Experimental

### 2.1. Chemicals and preparation of the zinc and diacid samples

Zinc porphyrins were synthesized by boiling corresponding free-base porphyrin [20] with zinc acetate in a CH<sub>2</sub>Cl<sub>2</sub>/methanol solution (volume ratio: 2:1). The zinc porphyrin thus obtained was purified on a silica gel column with chloroform as the eluant

\* Corresponding author. Fax: +86 22 2350 8841.

E-mail address: [zhangyhi@nankai.edu.cn](mailto:zhangyhi@nankai.edu.cn) (Y.-H. Zhang).



MTPP:  $R_1=R_2=R_3=R_4=\text{phenyl}$

MTrPP:  $R_1=H, R_2=R_3=R_4=\text{phenyl}$

MDPP:  $R_1=R_3=H, R_2=R_4=\text{phenyl}$

MMPP:  $R_1=R_2=R_3=H, R_4=\text{phenyl}$

MP:  $R_1=R_2=R_3=R_4=H$

$M=\text{Zn}, H_4$

**Fig. 1.** Labeling diagram of porphyrins and polarization direction of molecular excitation.

and then dissolved in chloroform for measurement of absorption spectra. Diacid species were prepared by solving corresponding free-base porphyrins with aqueous HCl (12 mol/L)/ethanol/ $\text{CH}_2\text{Cl}_2$  solution (volume ratio 1:10:50), or with a  $\text{CF}_3\text{COOH}/\text{CH}_2\text{Cl}_2$  solution (volume ratio 1:20). A UV–vis spectrometer was employed to ensure complete conversion of free-base porphyrin to zinc complexes or diacid species. The concentration of the sample used for UV–vis absorption spectra measurement was  $5 \times 10^{-6}$  mol/L. Such low concentrations do not usually generate measurable aggregation. All reagents (AR grade) were used without further treatment.

Absorption spectra were recorded on a Shimadzu UV-2450 absorption spectrophotometer.

## 2.2. Computational methods

Structural optimization and TDDFT calculation were carried out at B3LYP [21,22] and PBE1PBE [23] levels by using a 6-31G(d) basis set for C, H, N, and Cl atoms, and LanL2DZ basis set for the Zn atom. A similar theoretical level has been recently used in studies of the hydrogen bond in porphyrin diacids [12] and electronic structure of zinc porphyrins [24]. For comparison, calculations at the PBEPBE [25] level were also carried out by using the SVP basis sets for all atoms. All calculations were performed with the Gaussian 03 suite of programs [26]. Simulated UV–vis spectra were derived, from a Gaussian output file using the SWizard program (revision 4.6 [27]), in Gaussian line shape with a half-bandwidth of  $1000 \text{ cm}^{-1}$ .

In the literature [18], there have been reports that thorough analysis of the structural and spectroscopic properties of porphyrin diacids should consider the influence of conjugated bases

of the acid used because of the close interaction between two moieties in solution as well as in the solid state; however, the study of  $\text{H}_4\text{P}^{2+}$  without consideration of counterion has also been reported [28]. Similarly, our calculations in the present study also reveal marked difference in spectral structure between calculation with and without consideration of  $\text{Cl}^-$  ion for *meso*-phenylporphyrin diacids. The predicted spectra of the former scenario coincide better with the experiment than the latter scenario. The normal-coordinate structural decomposition (NSD) data were obtained by online calculation utilizing the NSD Computation Engine (version 3.0) provided on the Website of the Shelmutt group [29].

## 3. Results and discussion

### 3.1. The geometric structure of porphyrin diacids

Optimization of the geometric structure of zinc porphyrin by application of the B3LYP method has been reported in a previous study [30]; the general conclusion was that the in-plane distortion caused by the *meso*-phenyl substitution is significant, whereas the out-of-plane distortion is slight. New calculation with the PBE1PBE/6-31G(d)/LanL2DZ (see Table 1), B3LYP/6-31G(d)/LanL2DZ (see Table S1), and PBEPBE/SVP methods (see Table S2) generate similar results. The crystal data [31] and calculation data, reported by another group of researchers [32], for ZnTPP are also listed in Table 1 for comparison.

The structural parameters of HCl-acidified porphyrin diacids optimized by the PBE1PBE/6-31G(d) method are summarized in Table 2, wherein the X-ray data [33] and the calculated data of  $\text{H}_4\text{TPP}^{2+}(\text{Cl}^-)_2$  [21] reported by other groups of researchers are provided for comparison. The results of our calculation predict a geometric structure similar to that reported in the published literature [21], with the exception of slight differences pertaining to the  $\text{Cl}^- \cdots \text{H}-\text{N}$  hydrogen bond. For all porphyrin diacids, the saddling structure is predicted to be the most stable, and this is in accordance with the literatures [16–19]. Among all the structural features of the porphyrin diacids, the most noticeable feature is the significant out-of-plane distortion of the porphyrin ring that increases successively with the extent of *meso*-phenyl substitution. The  $\text{H}_4\text{DPP}^{2+}(\text{Cl}^-)_2$  displays larger out-of-plane distortion than the  $\text{H}_4\text{MPP}^{2+}(\text{Cl}^-)_2$ , which differs from the observation reported in the literature [19], where diarylporphyrin diacid is less distorted than monoarylporphyrin diacid. This discrepancy could be ascribed to the differences in molecular environment.

We estimated the NSD of zinc porphyrins and porphyrin diacids on the basis of stable geometry optimized by PBE1PBE methods (see Table S3). The total out-of-plane distortion (DOOP) of porphyrin diacids ( $>1.5 \text{ \AA}$ ) is, in general, predicted to be larger than that of zinc porphyrins ( $<0.40 \text{ \AA}$ ). Further,  $B_{2u}$  modes (saddling vibration) are predicted to contribute significantly to DOOP for all porphyrins studied here, whereas  $B_{1u}$  modes (ruffling vibration) that usually display marked out-of-plane displacement in ruffled porphyrin display negligible displacement in this study. In addition to the  $1B_{2u}$  mode, the  $2B_{2u}$  mode also displays moderate out-of-plane displacement ( $>0.2 \text{ \AA}$ ). Based on NSD analysis, out-of-plane distortion is expected to generate a larger spectral redshift for porphyrin diacids than for zinc complexes.

Another noticeable feature of diacid species is the lower twisting orientation of the *meso*-phenyl group relative to the mean-plane of porphyrin ring. The dihedral ( $<43^\circ$ ) between the *meso*-phenyl and the mean plane of the porphyrin ring, predicted to decrease with the extent of *meso*-phenyl substitution, is much smaller than that of zinc complexes ( $>62^\circ$ ). The nearly co-planar orientation of the *meso*-phenyl group with regard to porphyrin is believed to enhance

**Table 1**

Calculated structural parameters of zinc porphyrins skeleton by the PBE1PBE/6-31G(d)/LanL2DZ method.

	ZnTPP			ZnTrPP	ZnDPP	ZnMPP	ZnP
	Exp <sup>a</sup>	Cal <sup>b</sup>	Cal <sup>c</sup>				
<b>Bond length (Å)</b>							
C <sub>β</sub> –C <sub>β</sub>	1.349	1.361	1.360	1.360–1.361	1.361	1.364–1.365	1.362
C <sub>α</sub> –C <sub>β</sub>	1.440	1.446	1.442	1.439–1.445	1.439–1.446	1.439–1.445	1.442
C <sub>α</sub> –N	1.376	1.376	1.368	1.365–1.368	1.366–1.367	1.364–1.367	1.365
C <sub>α</sub> –C <sub>m</sub>	1.400	1.408	1.407	1.394–1.409	1.395–1.408	1.394–1.409	1.396
N–Zn	2.037	2.055	2.059	2.058–2.060	2.058	2.057–2.058	2.057
C <sub>5</sub> ···C <sub>15</sub>		6.926	6.905	6.931	6.954	6.903	6.852
C <sub>20</sub> ···C <sub>10</sub>		6.926	6.905	6.854	6.801	6.827	
<b>Angle (degree)</b>							
∠C <sub>α</sub> C <sub>m</sub> C <sub>α</sub>		125.1	125.3	125.1–127.4	124.9–127.6	125.1–127.3	127.1
∠NC <sub>α</sub> C <sub>β</sub>	109.4	109.4	109.4	109.4–109.7	109.3–109.7	109.3–109.6	109.5
∠C <sub>α</sub> C <sub>β</sub> C <sub>β</sub>	107.4	107.1	107.0	106.9–107.0	~106.9	106.8–106.9	106.9
∠C <sub>α</sub> NC <sub>α</sub>	106.6	107.0	107.2	107.1–107.2	107.2	107.2–107.3	107.2
<b>Dihedral (degree) and out-of-plane displacement (Å)</b>							
NC <sub>α</sub> C <sub>m</sub> C <sub>α</sub>			3.369	1.859–3.693	1.199–1.406	0.083–1.308	0.000
Ph–Por. <sup>d</sup>			62.42	61.91–62.4	64.48	65.34	
Δ <sub>total</sub>			1.513	1.265	0.523	0.291	0.000
ΔC <sub>β</sub>			0.146	0.085–0.153	0.048–0.054	0.003–0.051	0.000

<sup>a</sup> Experimental data from Ref. [31].<sup>b</sup> Calculated data from Ref. [32].<sup>c</sup> Calculated data from the present study.<sup>d</sup> The dihedral between phenyl plane and the mean-plane of porphyrins.

the π-electron delocalization effect between two moieties in a porphyrin diacid.

With regard to in-plane distortion, the variation upon *meso*-phenyl substitution is similar to that observed in zinc porphyrins. The largest variation was also found in the vicinity of *meso*-C<sub>m</sub> atoms.

*meso*-Phenyl substitution also induces noticeable variation in hydrogen bond configuration. The Cl···H distance is increased and the H–N bond is shortened; this indicates that the Cl···H–N hydrogen bond is weakened by *meso*-phenyl substitution.

Both B3LYP and PBEPBE calculations generate similar geometric variations for porphyrin diacids (see Tables S4 and S5) as compared with the PBE1PBE calculation.

### 3.2. Electronic structure of zinc complex and diacid species of porphyrins

Tables 3 and 4 summarize, respectively, the ground-state electronic level predicted by the PBE1PBE method for zinc porphyrins and porphyrin diacids.

#### 3.2.1. Zinc porphyrins

Review of the data presented in Table 3 reveals two noticeable variations of frontier orbitals with *meso*-phenyl substitution: (1) the orbital level is elevated for HOMO, HOMO–1, and averaged LUMO/LUMO+1 orbitals by *meso*-phenyl substitution; this is attributable to a higher energy level of the phenyl group than

**Table 2**

Optimized structural parameter of porphyrin diacids by PBE1PBE/6-31G(d) calculation.

	H <sub>4</sub> TPP <sup>2+</sup> (Cl <sup>-</sup> ) <sub>2</sub> (D <sub>2d</sub> )			H <sub>4</sub> TrPP <sup>2+</sup> (Cl <sup>-</sup> ) <sub>2</sub> (C <sub>2</sub> )	H <sub>4</sub> DPP <sup>2+</sup> (Cl <sup>-</sup> ) <sub>2</sub> (D <sub>2</sub> )	H <sub>4</sub> MPP <sup>2+</sup> (Cl <sup>-</sup> ) <sub>2</sub> (C <sub>2</sub> )	H <sub>4</sub> P <sup>2+</sup> (Cl <sup>-</sup> ) <sub>2</sub> (D <sub>2d</sub> )
	Exp <sup>a</sup>	Cal <sup>b</sup>	Cal <sup>c</sup>				
<b>Bond length (Å)</b>							
C <sub>β</sub> –C <sub>β</sub>	1.366	1.369	1.365	1.364–1.365	1.368	1.364–1.365	1.364
C <sub>α</sub> –C <sub>β</sub>	1.431	1.435	1.432	1.433–1.437	1.433–1.436	1.432–1.437	1.436
C <sub>α</sub> –N	1.390	1.373	1.364	1.363–1.365	1.363–1.364	1.362–1.364	1.363
C <sub>α</sub> –C <sub>m</sub>	1.414	1.414	1.408	1.394–1.413	1.394–1.408	1.391–1.409	1.395
N–H		1.074	1.054	1.054–1.056	1.055	1.055–1.057	1.056
H···Cl		1.973	2.020	2.002–2.022	2.006	1.994–2.011	1.999
N···Cl		3.044	3.069	3.053–3.065	3.050	3.040–3.049	3.040
C <sub>5</sub> ···C <sub>15</sub>			6.926	6.845	6.766	6.815	6.880
C <sub>20</sub> ···C <sub>10</sub>			6.926	6.988	7.042	6.971	6.880
<b>Angle (degree)</b>							
∠C <sub>α</sub> C <sub>m</sub> C <sub>α</sub>	123.2	124.1	124.0	124.0–127.6	123.9–128.3	124.4–128.0	127.5
∠NC <sub>α</sub> C <sub>β</sub>	106.1	107.5	107.5	107.4–107.6	107.4–107.6	107.4–107.6	107.5
∠C <sub>α</sub> C <sub>β</sub> C <sub>β</sub>	108.7	107.7	107.6	107.4–107.6	107.7–107.8	~107.6	107.6
∠C <sub>α</sub> NC <sub>α</sub>	110.3	109.6	109.8	109.8	109.8	109.8–109.9	109.9
∠NHX	165.0	174.3	173.3	169.9–173.1	169.8	167.4–170.3	167.8
<b>Dihedral (degree) and out-of-plane displacement (Å)</b>							
NC <sub>α</sub> C <sub>m</sub> C <sub>α</sub>			21.22	16.25–21.06	16.37–16.68	13.19–16.62	13.36
Ph–Por. <sup>d</sup>			35.43	37.97–39.28	42.46	42.95	0
Δ <sub>total</sub>			9.103	7.915	6.867	6.198	5.382
ΔC <sub>β</sub>	0.93	0.838	0.851	0.667–0.805	0.633–0.650	0.482–0.661	0.500

<sup>a</sup> Experimental data from Ref. [33].<sup>b</sup> Calculated data from Ref. [21].<sup>c</sup> Calculated data from the present study.<sup>d</sup> The dihedral between *meso*-phenyl plane and the mean-plane of porphyrins.

**Table 3**  
Predicted orbital energy of zinc porphyrins by the PBE1PBE/6-31G(d)/LanL2DZ method (in eV).

	ZnTPP (D <sub>2d</sub> )	ZnTrPP (C <sub>2</sub> )	ZnDPP (D <sub>2</sub> )	ZnMPP (C <sub>2</sub> )	ZnP (D <sub>4h</sub> )
LUMO+1	−2.1126 (e)	−2.1045 (b)	−2.0925 (b <sub>1</sub> )	−2.1012 (a)	−2.1134 (e <sub>g</sub> )
LUMO	−2.1126 (e)	−2.1221 (a)	−2.1276 (b <sub>2</sub> )	−2.1186 (b)	−2.1134 (e <sub>g</sub> )
HOMO	−5.1180 (b <sub>2</sub> )	−5.1794 (b)	−5.2556 (b <sub>3</sub> )	−5.3260 (b)	−5.3995 (a <sub>2u</sub> )
HOMO−1	−5.3755 (b <sub>1</sub> )	−5.3910 (a)	−5.4055 (a)	−5.4204 (a)	−5.4395 (a <sub>1u</sub> )
HOMO−LUMO	3.0054	3.0573	3.1230	3.2074	3.2861

the porphyrin moiety [18]. The largest elevation (~0.282 eV) is observed for the HOMO orbit, which reduces the HOMO–LUMO gap from 3.286 eV of ZnP to 3.005 eV of ZnTPP; (2) LUMO/LUMO+1 orbit, that degenerated in ZnP and ZnTPP, become nondegenerate and there is a substantially split in energy for asymmetric porphyrins. The greatest division is observed in ZnDPP (0.035 eV), and this is closely related to the maximum discrepancy between the configuration around H- and phenyl-suspended C<sub>m</sub> observed in ZnDPP.

These afore-described variations should be ascribed to the participation of the *meso*-phenyl group in Gouterman Four Orbits, particularly in the HOMO orbit (Fig. S1). Natural orbit population analysis indicates that the Gouterman-type HOMO orbit centers primarily on C<sub>m</sub> and N atoms and, therefore, is readily disturbed by *meso*-substitution. For example, the MO coefficient of C<sub>m</sub> and N atoms decreases from ~0.58 and ~0.27 in ZnP, respectively, to 0.46 and 0.21 in ZnTPP; however, the MO coefficient of the phenyl group increases. The HOMO−1 orbit is primarily centered on C<sub>α</sub> and C<sub>β</sub> atoms and, therefore, is subjected to less influence than the HOMO orbit. The splitting of LUMO/LUMO+1 orbit observed in asymmetric porphyrins (ZnMPP, ZnDPP, and ZnTrPP) should be attributed to the different numbers of *meso*-phenyl groups involved in these two orbit. LUMO and LUMO+1 orbit of ZnDPP involve zero and two *meso*-phenyl groups, respectively, this induces the maximum discrepancy in orbital composition and, therefore, produces the biggest division in energy for LUMO and LUMO+1 orbit.

The B3LYP calculation (Table S6) generates a similar electronic structure as that with the PBE1PBE method, whereas the PBEPBE method predicts a slightly higher energy for HOMO and HOMO−1 orbit, a marginally lesser energy for LUMO/LUMO+1 orbit and, consequently, a smaller HOMO–LUMO gap (Table S7).

### 3.2.2. Porphyrin diacids

The complexity of the electronic structure of H<sub>4</sub>P<sup>2+</sup>(Cl<sup>−</sup>)<sub>2</sub> and H<sub>4</sub>TPP<sup>2+</sup>(Cl<sup>−</sup>)<sub>2</sub>, caused by the insertion of the Cl<sup>−</sup> lone pair orbit, has been revealed in the published literature [17,18] and was also testified in our calculation in this study. Although LUMO/LUMO+1 orbit are nearly similar to that of zinc porphyrins, the ordering of occupied frontier orbit is observed to be significantly different from zinc porphyrins and is influenced by the calculation method

**Table 4**  
Calculated orbital energy of HCl-acidified porphyrins by the PBE1PBE/6-31G(d) method (in eV)<sup>a,b</sup>.

	H <sub>4</sub> TPP <sup>2+</sup> (Cl <sup>−</sup> ) <sub>2</sub>	H <sub>4</sub> TrPP <sup>2+</sup> (Cl <sup>−</sup> ) <sub>2</sub>	H <sub>4</sub> DPP <sup>2+</sup> (Cl <sup>−</sup> ) <sub>2</sub>	H <sub>4</sub> MPP <sup>2+</sup> (Cl <sup>−</sup> ) <sub>2</sub>	H <sub>4</sub> P <sup>2+</sup> (Cl <sup>−</sup> ) <sub>2</sub>
LUMO+1	2.8410	−2.8710	−2.9161	−2.9648	−3.0255
LUMO	2.8410	−2.8756	−2.9245	−2.9670	−3.0255
HOMO	5.3940 (G-HOMO)	−5.5431 (G-HOMO)	−5.6946 (G-HOMO)	−5.8328 (G-HOMO)	−5.9818 (G-HOMO)
HOMO−1	5.8298 (p)	−5.8779 (p)	−5.9307 (p)	−5.9794 (p)	−6.3704 (p)
HOMO−2	5.8298 (p)	−5.8779 (p)	−5.9331 (p)	−5.9835 (p)	−6.3704 (p)
HOMO−3	6.0727 (G-HOMO−1)	−6.1029 (G-HOMO−1)	−6.1548 (G-HOMO−1)	−6.2060 (G-HOMO−1)	−6.2737 (G-HOMO−1)
HOMO−4	6.0942 (p)	−6.1532 (p)	−6.2220 (p)	−6.2723 (p)	−6.3300 (p)
HOMO−5	6.1216 (p)	−6.1717 (p)	−6.2269 (p)	−6.2745 (p)	−6.3300 (p)
HOMO−6	6.1216 (p)	−6.1760	−6.2277	−6.2818	−6.3439 (p)
HOMO−7	6.1320 (G-HOMO*)	−6.2155 (G-HOMO*)	−6.3139 (G-HOMO*)	−6.4132 (G-HOMO*)	−6.5481 (G-HOMO*)
(G-HOMO)−LUMO	2.5530	2.6675	2.7701	2.8658	2.9563

<sup>a</sup> p in parentheses denotes the p orbit of Cl atom.

<sup>b</sup> G-HOMO and G-HOMO−1 correspond to the Gouterman-type HOMO and HOMO−1 orbit, respectively, G-HOMO\* orbit has similar structure with G-HOMO but centers mainly on the Cl atom.

employed. By checking the electron orbital map (Fig. S2), the HOMO and HOMO−3 orbit of the PBE1PBE calculation are identified as the Gouterman-type HOMO and HOMO−1 orbit (abbreviated as G-HOMO and G-HOMO−1 orbit), respectively. The orbital ordering predicted by the B3LYP and PBEPBE methods (Tables S8 and S9) differs from that obtained from the PBE1PBE calculation and, further, is closely related to the *meso*-phenyl number.

There is another lower occupied MO in H<sub>4</sub>P<sup>2+</sup>(Cl<sup>−</sup>)<sub>2</sub>; this is located primarily on C<sub>m</sub>, N, and Cl atoms as the G-HOMO orbit but has different nodal features. This orbit was predicted to contribute predominantly to an excitation in the Q region with notable oscillator strength; therefore, it is labeled as the G-HOMO\* orbit in this study. The mixing of Cl<sup>−</sup> and porphyrin-based orbit within the G-HOMO and G-HOMO\* orbit reflects the interaction between the Cl<sup>−</sup> ion and the porphyrin ring that drives the formation of the Cl<sup>−</sup>·H–N hydrogen bond. It is apparent that G-HOMO and G-HOMO\* orbit display a contrary change trend following *meso*-phenyl substitution (Table 5 and Fig. S2). The G-HOMO orbit has a higher energy level and displays decreasing MO coefficient of Cl<sup>−</sup> ion and increasing coefficient of C<sub>m</sub> and N atoms; however, the converse is true for the G-HOMO\* orbit. This difference indicates that orbital mixing is reduced markedly by the *meso*-phenyl substitution that produces an almost pure Cl<sup>−</sup> and porphyrin-based orbit, respectively, for G-HOMO\* and G-HOMO in H<sub>4</sub>TPP<sup>2+</sup>(Cl<sup>−</sup>)<sub>2</sub>; this further proves that the Cl<sup>−</sup>·H–N hydrogen bond is weakened by the *meso*-phenyl substitution observed in structural analysis.

In general, the spectral shift correlates with the variation of the HOMO–LUMO gap [18]. For porphyrin diacids, although the level of the MO is uplifted by *meso*-phenyl substitution, the G-HOMO–LUMO gap is reduced from 2.9563 eV of H<sub>4</sub>P<sup>2+</sup>(Cl<sup>−</sup>)<sub>2</sub> to 2.5530 eV of H<sub>4</sub>TPP<sup>2+</sup>(Cl<sup>−</sup>)<sub>2</sub>; this is consistent with the observed redshift of electronic absorption (see Section 3.3).

### 3.2.3. Analysis of some influences to MO level

To evaluate the influence of conformational distortion, electron effect of *meso*-phenyl, and electronic effect of the Cl<sup>−</sup> ion on MO level, theoretical calculations were performed on several artificially adjusted porphyrin models (Table 6), and the obtained results are discussed in the following sub-sections.

**Table 5**

The calculated molecular orbit composition of G-HOMO and G-HOMO\* orbit by the PBE1PBE/6-31G(d) method.

		Molecular orbit coefficient <sup>a</sup>				
		H <sub>4</sub> TPP <sup>2+</sup> (Cl <sup>-</sup> ) <sub>2</sub>	H <sub>4</sub> TrPP <sup>2+</sup> (Cl <sup>-</sup> ) <sub>2</sub>	H <sub>4</sub> DPP <sup>2+</sup> (Cl <sup>-</sup> ) <sub>2</sub>	H <sub>4</sub> MPP <sup>2+</sup> (Cl <sup>-</sup> ) <sub>2</sub>	H <sub>4</sub> P <sup>2+</sup> (Cl <sup>-</sup> ) <sub>2</sub>
G-HOMO	C <sub>m</sub>	0.405	0.412	0.414	0.398	0.376
	N	0.227	0.247	0.269	0.283	0.302
	Ph <sup>b</sup>	0.234	0.179	0.124	0.062	0.000
	Cl	0.033	0.067	0.22	0.186	0.269
G-HOMO*	C <sub>m</sub>	0.044	0.022	0.020	0.071	0.144
	N	0.085	0.081	0.078	0.072	0.890
	Ph <sup>b</sup>	0.012	0.017	0.021	0.019	0.000
	Cl	0.791	0.764	0.726	0.627	0.597
G-HOMO <sup>c</sup>	C <sub>m</sub>	0.308	0.308	0.290	0.286	
	N	0.122	0.118	0.110	0.104	
	Ph <sup>b</sup>	0.362	0.349	0.375	0.359	

<sup>a</sup> Normalized to 1.<sup>b</sup> Phenyl group.<sup>c</sup> The orbit of **ad-porphyrin III** series.**Table 6**The collection of artificially adjusted porphyrin models<sup>a,b</sup>.

	Porphyrin diacids			Zinc porphyrins <sup>c</sup>		
	Cl ion	Phenyl group	Effects <sup>d</sup>	Zinc ion	Phenyl group	Effects <sup>d</sup>
<b>Ad-porphyrin I</b>	×	×	A			
<b>Ad-porphyrin II</b>	✓	×	A+B	✓	×	A
<b>Ad-porphyrin III</b>	×	✓	A+C			
<b>Ad-porphyrin IV<sup>e</sup></b>	✓	✓	A+B+C <sup>f</sup>	✓	✓	A+C <sup>f</sup>
Parent series	✓	✓	A+B+C	✓	✓	A+C

<sup>a</sup> All porphyrin models are deduced from parent porphyrin without further optimization.<sup>b</sup> "✓" indicates involved while "×" indicates eliminated.<sup>c</sup> For adjusted zinc porphyrins, only **ad-porphyrin II** and **IV** series are constructed.<sup>d</sup> "A" indicates conformational effect; "B" indicates electronic effect of counterion Cl<sup>-</sup>; and "C" indicates electronic effect of *meso*-phenyl group.<sup>e</sup> In which phenyl plane is adjusted to a perpendicular orientation with respect to the mean plane of porphyrin ring.<sup>f</sup> Only electronic donating effect is involved.

(1) *Conformational distortion*. The replacement of the *meso*-phenyl by the H atom with the simultaneous extrusion of the Cl<sup>-</sup> ion produces the first type of an adjusted porphyrin model (**ad-porphyrin I** series); in this model, only the influence of con-

formational distortion is retained. The electron orbital level of **ad-porphyrin I** is presented in Table 7. In comparison with the parent porphyrin diacid, the **ad-porphyrin I** displays a much lower MO level, due to the exclusion of the *meso*-phenyl group and cen-

**Table 7**

Calculated orbital energy of several adjusted porphyrin diacid series by the PBE1PBE/6-31G(d) method (in eV).

	H <sub>4</sub> TPP <sup>2+</sup> (Cl <sup>-</sup> ) <sub>2</sub>	H <sub>4</sub> TrPP <sup>2+</sup> (Cl <sup>-</sup> ) <sub>2</sub>	H <sub>4</sub> DPP <sup>2+</sup> (Cl <sup>-</sup> ) <sub>2</sub>	H <sub>4</sub> MPP <sup>2+</sup> (Cl <sup>-</sup> ) <sub>2</sub>	H <sub>4</sub> P <sup>2+</sup> (Cl <sup>-</sup> ) <sub>2</sub>	δ <sup>a</sup>
<b>Ad-porphyrin I</b>						
LUMO+1	-9.6590	-9.6383	-9.6258	-9.6329	-9.6427	
LUMO	-9.6590	-9.6582	-9.6636	-9.6552	-9.6427	
G-HOMO	-12.7318	-12.7633	-12.7949	-12.8205	-12.8479	
G-HOMO-1	-12.8876	-12.8860	-12.8879	-12.8923	-12.8972	
(G-HOMO)-LOMO	3.0728	3.1052	3.1313	3.1653	3.2053	0.1325
<b>Ad-porphyrin II</b>						
LUMO+1	-3.0586	-3.0399	-3.0181	-3.0208	-3.0255	
LUMO	-3.0586	-3.0608	-3.0641	-3.0467	-3.0255	
G-HOMO	-5.9824	-5.9862	-5.9903	-5.9845	-5.9818	
G-HOMO-1	-6.2557	-6.2560	-6.2631	-6.2672	-6.2737	
G-HOMO*	-6.3830	-6.4309	-6.4752	-6.5114	-6.5481	
(G-HOMO)-LOMO	2.9237	2.9254	2.9262	2.9376	2.9537	0.0299
<b>Ad-porphyrin III</b>						
LUMO+1	-8.3915	-8.6031	-8.8683	-9.2162	-9.6427	
LUMO	-8.3915	-8.6836	-9.0386	-9.3084	-9.6427	
G-HOMO	-10.7160	-11.1164	-11.5290	-12.0308	-12.8479	
G-HOMO-1	-11.6460	-11.8374	-12.3532	-12.5999	-12.8972	
(G-HOMO)-LOMO	2.3245	2.4325	2.4855	2.7225	3.2053	0.8807
<b>Ad-porphyrin IV</b>						
LUMO+1	-2.8508				-3.0255	
LUMO	-2.8508				-3.0255	
G-HOMO	-5.6513				-5.9818	
G-HOMO-1	-6.0702				-6.2737	
(G-HOMO)-LOMO	2.8005				2.9563	0.1558

<sup>a</sup> The difference of (G-HOMO)-LOMO gap between the derivatives of H<sub>4</sub>TPP<sup>2+</sup>(Cl<sup>-</sup>)<sub>2</sub> and H<sub>4</sub>P<sup>2+</sup>(Cl<sup>-</sup>)<sub>2</sub> in each adjusted series.

tral  $\text{Cl}^-$  ion. Following *meso*-phenyl substitution, the level of the MO, in particular for the G-HOMO, increases successively due to increase in out-of-plane distortion. However, the variation step of the G-HOMO–LUMO gap from the derivative of  $\text{H}_4\text{P}^{2+}(\text{Cl}^-)_2$  to that of  $\text{H}_4\text{TPP}^{2+}(\text{Cl}^-)_2$  (0.1325 eV) is less than that of parent porphyrin diacids (0.4033 eV); this indicates that the conformational distortion is not the primary cause for the variation in the electronic structure of the porphyrin diacid series.

(2) *Electronic effect of central  $\text{Cl}^-$  ion.* The replacement of only the *meso*-phenyl group of the parent porphyrin by a hydrogen atom produces the second type of artificially adjusted porphyrin (**ad-porphyrin II**); this porphyrin possesses conformational and electronic effects of the  $\text{Cl}^-$  ion. By comparing **ad-porphyrin II** with **ad-porphyrin I**, we clarify the influence of the  $\text{Cl}^-$  ion on the MO level. In the calculation, **ad-porphyrin II** has a higher MO level, particularly G-HOMO orbit, than the **ad-porphyrin I** (Table 7); this is primarily attributed to the much higher orbital level of the  $\text{Cl}^-$  ion than that of the porphyrin unit [34]. However, the G-HOMO–LUMO gap, as well as its variation step (0.0299 eV) with extension of *meso*-phenyl substitution, is less than that in **ad-porphyrin I**. This indicates that consideration of  $\text{Cl}^-$  in the calculation would diminish the variation step of the G-HOMO–LUMO gap because of the reduced interaction between  $\text{Cl}^-$  and porphyrin ring with increase in the extent of *meso*-phenyl substitution.

(3) *Electronic effect of meso-phenyl group.* The third type of adjusted porphyrins, **ad-porphyrin III**, is constructed by omission of the central  $\text{Cl}^-$  ion of the parent series. Both conformational and electronic effects of the *meso*-phenyl group are involved in this series.

Similar to the observation in zinc porphyrins, the *meso*-phenyl substitution uplifts the MO level, particularly the G-HOMO level (Table 7), because of a higher MO level of phenyl than the porphyrin moiety [18]. The G-HOMO–LUMO gap of **ad-porphyrin III**, although smaller than that of **ad-porphyrin I**, displays a larger variation step (0.8807 eV) than that of **ad-porphyrin I**. The pure electronic effect of *meso*-phenyl substitution can reasonably be evaluated by comparing the variation of the G-HOMO–LUMO gap in the **ad-porphyrin I** with that in the **ad-porphyrin III** series; the difference of the variation step between **ad-porphyrin I** and **III** series (0.7482 eV) could be ascribed to the electronic effect of *meso*-phenyl group. This step is greater than the one observed in **ad-porphyrin I**, which indicates that the electronic effect of the *meso*-phenyl group has a much greater influence on electronic structure than conformational distortion does for the porphyrin diacid.

If considering the  $\text{Cl}^-$  in calculation, the electronic effect of *meso*-phenyl substitution could be evaluated by comparison of the **ad-porphyrin II** series with the parent porphyrin diacid; this predicts a contribution of 0.3734 eV for the electronic effect of the *meso*-phenyl group to the variation in the G-HOMO–LUMO gap. This value is approximately half of the 0.7482 eV value obtained in the calculation without considering the  $\text{Cl}^-$  ion, and can be interpreted in terms of competition between counterion  $\text{Cl}^-$  and the *meso*-phenyl group in the electron-donating effect to the porphyrin ring. The electron donating effect of the counterion decreases with increase in the extent of *meso*-phenyl substitution because of a weakened  $\text{Cl}^- \cdots \text{H}-\text{N}$  hydrogen bond. Therefore, we conclude that the influence of each factor overlaps with that of other factors; this accounts for the abnormal lesser variation of the G-HOMO–LUMO gap (0.4033 eV) observed in the parent diacid series instead of the 0.8807 eV of the **ad-porphyrin III** series. The overlapping of the electronic effect of the *meso*-phenyl group and the counterion  $\text{Cl}^-$  is also demonstrated by comparison of MO population between the parent porphyrin diacid series and **ad-porphyrin III** series (Table 5). Data presented in Table 5 indicate that the MO coefficient of the phenyl group in the G-HOMO orbit of the parent series is

increased nearly in a directly proportional manner with the extension of *meso*-phenyl number. However, this increase is significantly obliterated in the **ad-porphyrin III** series, where the MO coefficient of the *meso*-phenyl group is observed to be almost constant for all porphyrin diacids.

The electronic effect of the *meso*-phenyl group can be further divided into an electron-donating and  $\pi$ -electron delocalization effects. These two effects can be differentiated by comparison of parent porphyrin diacids with **ad-porphyrin IV** series, wherein the *meso*-phenyl group is adjusted to be perpendicular to the porphyrin ring. This configuration maximally diminishes the  $\pi$ -electron delocalization between the *meso*-phenyl and porphyrin rings. A comparison of the **ad-porphyrin IV** with the parent porphyrin diacid predicts a contribution of 0.1259 eV for the electronic donating effect; therefore, this spares 0.2475 eV for the delocalization effect to the variation of the G-HOMO–LUMO gap (Table 7). A similar comparison was also performed without consideration of  $\text{Cl}^-$ , that is, a comparison between **ad-porphyrin III** series and its corresponding further-adjusted series with perpendicular *meso*-phenyl groups; the comparison predicted a contribution of 0.3832 and 0.3650 eV, respectively, for electron-donating and  $\pi$ -delocalization effects. Therefore, we conclude that consideration of  $\text{Cl}^-$  in calculations would reduce the influence of the electron-donating effect of the *meso*-phenyl group more significantly than that of the delocalization effect, and this is attributed to the competitive electron-donating effect of the  $\text{Cl}^-$  ion.

### 3.3. Absorption spectra

#### 3.3.1. Experimental spectra

Fig. 2 depicts experimental UV–vis spectra of zinc porphyrins in chloroform solution, and spectral data are summarized in Table 8. From Fig. 2 and Table 8, we infer that both B and Q bands undergo successive redshift following *meso*-phenyl substitution. The total shift distance for both B and  $Q_0$  band from ZnP to ZnTPP (25 nm) is comparable to that of the corresponding free-base species [20].

The absorption spectra of HCl-acidified porphyrin diacids are displayed in Fig. 3, and the observed spectral data accord well with that reported in the published literature [18,19]. For comparison, the spectra of  $\text{CF}_3\text{COOH}$ -acidified porphyrin diacids were recorded (Fig. S3). With the exception of slight differences in absorption wavelength due to different acid and solvent used, the redshift trend of B and Q bands with *meso*-phenyl substitution is observed to be similar for these two series of porphyrin diacids. In general, the redshift extent in the porphyrin diacid series that is caused by *meso*-phenyl substitution is greater than that observed in the zinc porphyrin series. For example, the redshift step of the B band of HCl-acidified porphyrin, measuring 36.5 nm, is at least 1.5-times larger than that of zinc porphyrins; however, the redshift step of the Q band (60.4 nm for  $Q_1$  and 79.7 nm for  $Q_0$  band) is approximately 2.5 times larger than that of zinc porphyrins. In addition, the  $Q_0$  band, which appears only as a weak shoulder in the right side of strong  $Q_1$  band in  $\text{H}_4\text{P}^{2+}(\text{Cl}^-)_2$ , is enhanced markedly by *meso*-phenyl substitution with regard to B and  $Q_1$  band.

#### 3.3.2. Theoretical simulation of absorption spectra

3.3.2.1. *Zinc porphyrins.* For zinc porphyrins, the excitation structure predicted by the PBE1PBE method could be explained well by the Gouterman Four Orbit model. The first four excitations predicted involve almost pure electron transition occurring between the Gouterman-type HOMO/HOMO–1 and LUMO/LUMO+1 orbitals; therefore, they are easily assigned to the Q and B bands (Table 8 and Tables S10–S14). The simulated redshift of B and Q band is consistent with the experimental results.

Detailed analysis of PBE1PBE calculation reveals certain notable features:

**Table 8**

Calculated excitation energy, oscillator strength ( $f$ ), and composition determined by the PBE1PBE/6-31G(d)/LanL2DZ method and experimental wavelength (in CHCl<sub>3</sub>) of B and Q bands of zinc porphyrins.

		Exp. (nm)	Cal.					
				Excitation nm (eV)	$f$	One-electron transition (weight)		
ZnTPP	B	419.0	B	374.4 (3.31)	1.4177	H-1 → L+1(+41%)	H-0 → L+0(22%)	
				374.4 (3.31)	1.4186	H-1 → L+0(+41%)	H-0 → L+1(+22%)	
	Q <sub>0</sub>	584.0	Q	535.8 (2.31)	0.0282	H-0 → L+1(+61%)	H-1 → L+0(43%)	
				535.8 (2.31)	0.0283	H-0 → L+0(+61%)	H-1 → L+1(+43%)	
ZnTrPP	B	413.0	B <sub>x</sub>	368.4 (3.37)	1.5495	H-1 → L+1(+40%)	H-0 → L+0(22%)	
			B <sub>y</sub>	367.0 (3.38)	1.1023	H-1 → L+0(+38%)	H-0 → L+1(+24%)	
	Q <sub>0</sub>	578.0	Q <sub>x</sub>	527.6 (2.35)	0.0249	H-0 → L+0(+60%)	H-1 → L+1(+44%)	
			578.0	Q <sub>y</sub>	527.1 (2.35)	0.0068	H-0 → L+1(+59%)	H-1 → L+0(46%)
ZnDPP	B	407.0	B <sub>x</sub>	352.4 (3.44)	1.7088	H-1 → L+1(+38%)	H-0 → L+0(+23%)	
			B <sub>y</sub>	351.0 (3.46)	0.7948	H-1 → L+0(+34%)	H-0 → L+1(26%)	
	Q <sub>0</sub>	570.0	Q <sub>x</sub>	517.6 (2.40)	0.0180	H-0 → L+0(+59%)	H-1 → L+1(46%)	
			570.0	Q <sub>y</sub>	517.4 (2.40)	0.0000	H-0 → L+1(+56%)	H-1 → L+0(+50%)
ZnMPP	B	401.0	B <sub>x</sub>	360.5 (3.44)	1.3279	H-1 → L+1(+34%)	H-0 → L+0(25%)	
			B <sub>y</sub>	359.3 (3.45)	0.8650	H-1 → L+0(+32%)	H-0 → L+1(+26%)	
	Q <sub>0</sub>	564.0	Q <sub>y</sub>	509.4 (2.43)	0.0004	H-0 → L+1(+54%)	H-1 → L+0(51%)	
			564.0	Q <sub>x</sub>	509.2 (2.44)	0.0015	H-0 → L+0(+56%)	H-1 → L+1(+49%)
ZnP	B	394.0	B	343.5 (3.61)	0.9664	H-1 → L+1(+23%)	H-0 → L+0(20%)	
				343.5 (3.61)	0.9664	H-1 → L+0(+8%)	H-0 → L+1(+7%)	
	Q <sub>0</sub>	559.0	Q				H-1 → L+0(+23%)	H-0 → L+1(+20%)
							H-1 → L+1(8%)	H-0 → L+0(+7%)
							H-0 → L+1(+46%)	H-1 → L+0(45%)
							H-0 → L+0(+7%)	H-1 → L+1(+7%)
			501.7 (2.47)	0.0014	H-0 → L+0(+46%)	H-1 → L+1(+45%)		
			501.7 (2.47)	0.0014	H-0 → L+1(7%)	H-1 → L+0(+7%)		

- (1) The contribution weight of electronic transition from HOMO and HOMO–1 orbit is different for the B and Q bands. The Q band receives slightly more contribution from the HOMO orbit, whereas the B band receives its contribution primarily from the HOMO–1 orbit. This nonuniform transition can be ascribed to the lifting of nearly degenerated HOMO and HOMO–1 orbitals that is caused by the *meso*-phenyl substitution.
- (2) The degenerated transition B<sub>x</sub>/B<sub>y</sub> and Q<sub>x</sub>/Q<sub>y</sub> (the polarized direction of  $x$  and  $y$  excitation; Fig. 1) observed in ZnP and ZnTPP are predicted to split in the asymmetric porphyrin, and the split size of the B band (>1.0 nm) is greater than that of the Q band (<0.5 nm). It is notable that calculation indicates that the polarized direction of zinc and diacid derivatives of porphyrin does not bisect the pyrrolic rings along either the N–N or N–HH–N axis as observed in free-base porphyrins, but, instead, goes through the *meso*-position.

The split of absorption can be attributed to the lifting of the degenerated LUMO/LUMO–1 orbit caused by unsymmetrical *meso*-phenyl substitution. For the B<sub>x</sub>/B<sub>y</sub> pair of asymmetric porphyrin, the excitation component involving a greater number of *meso*-phenyl groups in a polarized direction is predicted to possess lower excitation energy; this coincides with the general redshift of the B band upon *meso*-phenyl substitution. Consistent with this analysis, the greatest division of the B band is observed in ZnDPP ( $\Delta = 2.7$  nm). However, the case of Q band is ambiguous; there is no general rule defining the ordering of the Q<sub>x</sub>/Q<sub>y</sub> pair. The predicted oscillator strength also correlates with the *meso*-phenyl number for both B and Q bands. The component involving more number of *meso*-phenyl groups in the polarized direction is predicted to possess greater oscillator strength. Therefore, the ZnDPP displays the biggest difference in oscillator strength between two polarized components for both B and Q bands.

The dependence of calculated absorption wavelength on the *meso*-phenyl number is compared with experimental data in Fig. 4. From Fig. 4, it can be observed that the TDDFT calculation, although systematically overestimating the excitation energy, pre-

dicts similar variation trends for B and Q bands with the extent of *meso*-phenyl substitution. It should be emphasized that the direct comparison between calculated absorption wavelength and experimental data is impractical because of differences in molecular environment; however, the study of redshift trends of absorption band is much more meaningful. The B3LYP method provides a similar description of absorption spectra of zinc porphyrins (Tables S15–S19) with the PBE1PBE method, with the exception of a lesser overestimation of excitation energy.

The PBEPBE method predicts a markedly more complicated excitation structure (Tables S20–S24): (1) there are several excitations with moderate oscillator strength located in the B band region for asymmetric zinc porphyrins; (2) the electron transition from orbitals other than G–HOMO and G–HOMO–1 orbitals are observed to have notable, or a major contribution, to these excitations. Conversely, the case is simple for the Q band where only the Gouterman-type excitation is predicted to have notable oscillator strength. Fig. 4, further, indicates that the PBEPBE method, although producing a much closer absorption wavelength to that of the experiment by coincidence, predicts a less consistent variation with the experimental results for both B and Q bands, in comparison with the PBE1PBE and B3LYP methods.

**3.3.2.2. Porphyrin diacids.** The electronic structure of porphyrin diacid is described as deviating from the Gouterman Four Orbit model in the above-described data. Similarly, the excitation structure predicted by DFT methods cannot be fluently described by the Gouterman Four Orbit model (predicted excitation composition is summarized in Table 9 and Tables S25–S29 for the PBE1PBE method, Tables S30–S34 for the B3LYP method, and Tables S35–S39 for the PBEPBE method). The B band is easily identified because of its large oscillator strength, which is observed both in experiment and in theoretical calculation. However, the assignment of the Q band is confounded by the coexistence of two excitations, both of which have moderate oscillator strength in this region. The excitation with the higher excitation energy primarily involves the electron transition out of G–HOMO\*/G–HOMO–1 orbitals, and the other excitation

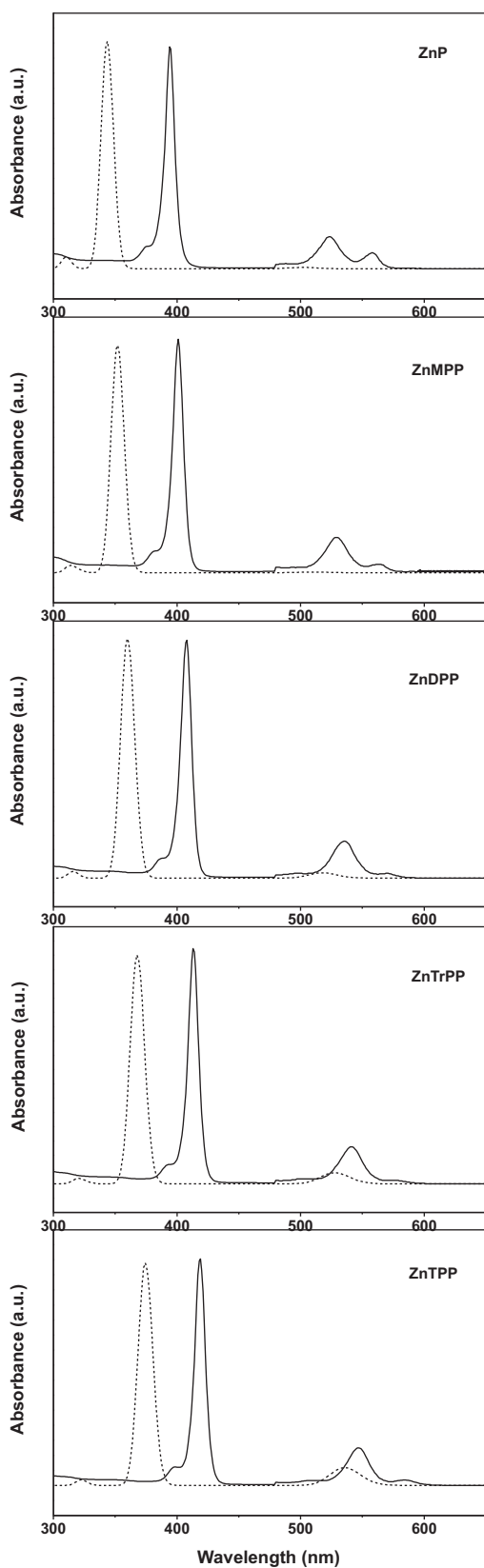


**Fig. 2.** Absorption spectra of zinc porphyrin (solid line: experimental spectra; dot line: calculated spectra by PBE1PBE/6-31G(d)/LanL2DZ method). The absorbance of spectra region (>480 nm) is multiplied by a factor of 4.

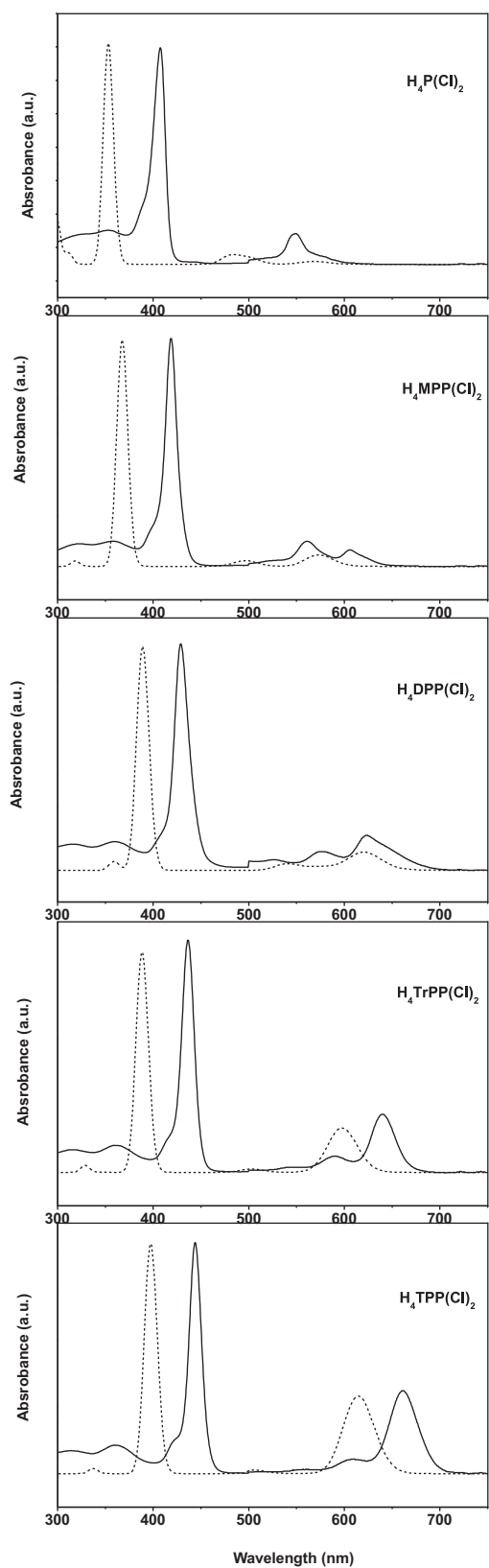


**Fig. 3.** Absorption spectra of HCl-acidified porphyrin (solid line: experimental spectra; dot line: calculated spectra by PBE1PBE/6-31G(d) method). The absorbance of spectra region (>500 nm) is multiplied by a factor of 3.

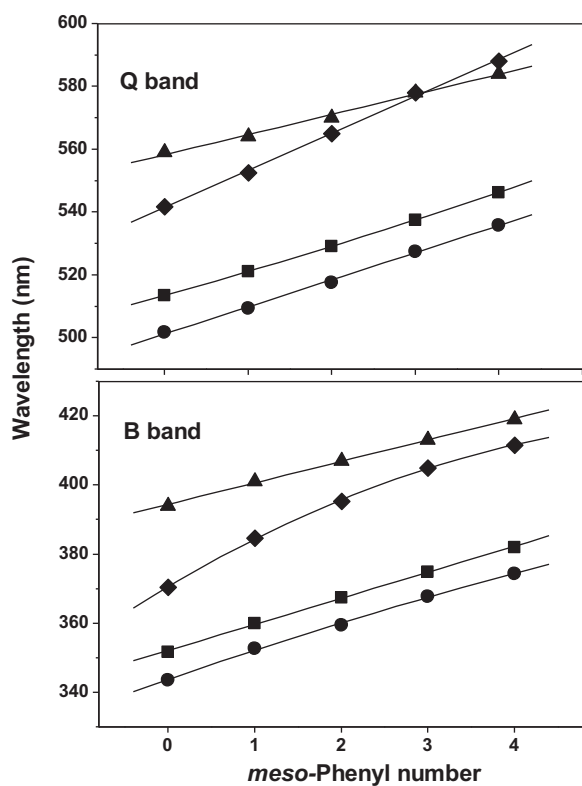


**Fig. 4.** Dependence of absorption wavelength (nm) on *meso*-phenyl number for zinc porphyrins (triangle: experimental data in chloroform solution; circle: calculated data by PBE1PBE/6-31G(d)/LanL2DZ method; quadrangle: calculated data by B3LYP/6-31G(d)/LanL2DZ method; diamond: calculated data by PBEPBE/SVP method).

with a lower excitation energy primarily involves electron transition out of G-HOMO/G-HOMO–1 orbit. Both PBE1PBE and B3LYP calculations predict that the latter excitation has greater oscillator strength and should be assigned to the Q absorption. This assignment is consistent with the general viewpoint with regard to Q absorption of porphyrins. However, the PBEPBE calculation generates a contrary assignment, similar to that suggested by Rosa [18] that the Q band receives a large contribution from the Cl-to-porphyrin transition.

The dependent profile of predicted absorption wavelength with *meso*-phenyl number is displayed in Fig. 5, where the PBE1PBE calculation predicts a profile that appears to be more consistent with experimental results than the other two DFT methods. Therefore, our discussion is mainly carried out on the basis of the PBE1PBE calculation.

Table 9 presents data indicating that the electron transition from the G-HOMO–1 orbit is predominantly for the B band, with increasing weight following *meso*-phenyl substitution. In addition, the G-HOMO\* orbit also contributes to the B band, but with a lesser and further decreasing transition with *meso*-phenyl substitution. In the Q band, the electron transition from G-HOMO is predominant, and the G-HOMO–1 orbit provides a moderate contribution.

From the zinc porphyrins, we observe that the PBEPBE method predicts an absorption wavelength that approximates better with the experimental results coincidentally. This was also observed for porphyrin diacids. However, the PBEPBE method has a less consistent variation profile when compared with the PBE1PBE method (Fig. 5). Further, the PBEPBE calculation provides a more complicated transition structure (Tables S35–S39) than the PBE1PBE and B3LYP methods: (1) in the B band, certain Cl-centered MOs, rather than G-HOMO\* and G-HOMO–1 orbitals, have dominant tran-

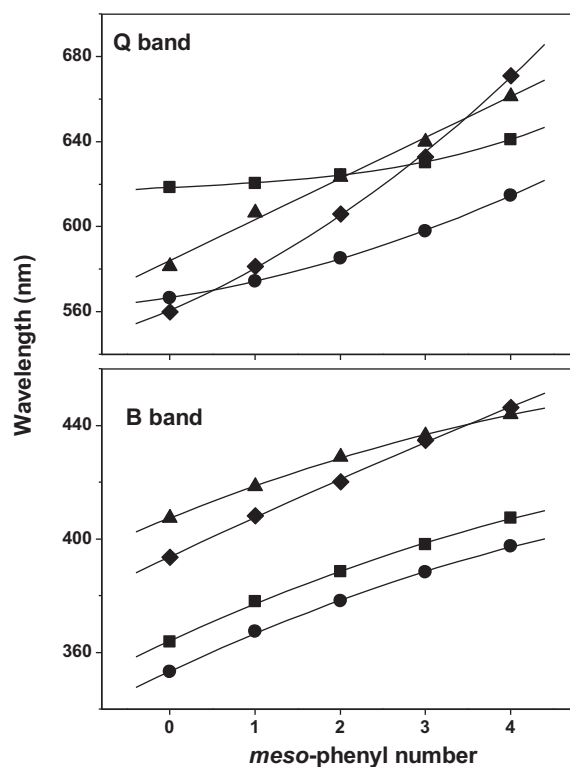


**Fig. 5.** Dependence of absorption wavelength (nm) on *meso*-phenyl number for HCl-acidified porphyrin diacids (triangle: experimental data in chloroform solution; quadrangle: calculated data by B3LYP/6-31G(d) method; circle: calculated data by PBE1PBE/6-31G(d) method; diamond: calculated data by PBEPBE/SVP method).

sition weight for  $H_4P^{2+}(Cl^-)_2$ ,  $H_4MPP^{2+}(Cl^-)_2$ , and  $H_4DPP^{2+}(Cl^-)_2$ ; (2) certain excitations involving electron transition from primarily HOMO–4/HOMO–5 to LUMO–2, not evident in the PBE1PBE and B3LYP calculations, are predicted to be located in the B band region with moderate oscillator strength. The spectral variation profile predicted by the PBEPBE method, although possessing a slightly larger slope, is similar to that predicted by the PBE1PBE and B3LYP methods.

In conclusion, the PBE1PBE method provides a more credible result than the B3LYP and PBEPBE methods in spectral simulation of diacid derivatives of *meso*-phenylporphyrin.

### 3.3.3. Analysis of the redshift of absorption bands

In this section, we attempt to allocate the total redshift of absorption to several important factors as well as to identify the key factor. The quantitative evaluation in the present study is performed on the basis of theoretical calculation of several artificially adjusted porphyrin models (Table 6). The TDDFT calculation results are presented in Tables S40 (PBE1PBE method) and S41 (B3LYP method), and the allocated results are summarized in Table 10.

**3.3.3.1. Zinc porphyrin series.** For zinc porphyrins, only the electronic and conformational effects are analyzed in this article; the influence of the hybrid orbital deformation (HOD) effect [10] has been ignored because of the negligible out-of-plane distortion. For both types of adjusted porphyrin models employed, **ad-porphyrins II** and **IV**, the central  $Zn^{2+}$  ion remained untouched. At first, the electronic effect of the *meso*-phenyl group and conformational effect could be differentiated by comparison of the TDDFT calculation of **ad-porphyrin II** series with that of the parent zinc porphyrins. Later, the electronic effect could be further differentiated into  $\pi$ -electron-delocalization and electron-donating effects

**Table 9**  
Calculated excitation energy, oscillator strength ( $f$ ), and composition determined by the PBE1PBE/6-31G(d) method and experimental wavelength of B and Q bands of HCl acidified porphyrins.

	Exp. (nm)		Cal.		One-electron transition (weight)		
			Excitation Nm (eV)	$f$			
H <sub>4</sub> TPP <sup>2+</sup> (Cl <sup>-</sup> ) <sub>2</sub>	B	444.0	B	397.4 (3.04)	1.2711	H-3 → L+1(+53%)	H-0 → L+0(+10%)
	Q <sub>0</sub>	661.9	Q	397.4 (3.04)	1.2709	H-3 → L+0(+53%)	H-0 → L+1(10%)
H <sub>4</sub> TrPP <sup>2+</sup> (Cl <sup>-</sup> ) <sub>2</sub>	B	436.5	B <sub>x</sub>	614.6 (2.17)	0.1433	H-0 → L+0(+71%)	H-3 → L+1(27%)
	Q <sub>0</sub>	639.9	Q <sub>y</sub>	614.6 (2.17)	0.1433	H-0 → L+1(+71%)	H-3 → L+0(+27%)
H <sub>4</sub> DPP <sup>2+</sup> (Cl <sup>-</sup> ) <sub>2</sub>	B	429.0	B <sub>x</sub>	388.7 (3.19)	1.4830	H-3 → L+0(+43%)	H-0 → L+1(+12%)
	Q <sub>0</sub>	639.9	B <sub>y</sub>	387.8 (3.20)	0.9587	H-3 → L+1(+43%)	H-0 → L+0(12%)
H <sub>4</sub> MPP <sup>2+</sup> (Cl <sup>-</sup> ) <sub>2</sub>	B	418.5	Q <sub>x</sub>	598.9 (2.07)	0.0538	H-0 → L+0(+70%)	H-3 → L+1(+25%)
	Q <sub>0</sub>	622.9	Q <sub>y</sub>	597.1 (2.08)	0.1083	H-0 → L+1(+70%)	H-3 → L+0(26%)
H <sub>4</sub> P <sup>2+</sup> (Cl <sup>-</sup> ) <sub>2</sub>	B	407.4	B <sub>x</sub>	379.3 (3.27)	1.7345	H-3 → L+0(+38%)	H-0 → L+1(+12%)
	Q <sub>0</sub>	605.0	B <sub>y</sub>	376.8 (3.29)	0.6287	H-3 → L+1(+38%)	H-0 → L+0(12%)
H <sub>4</sub> TPP <sup>2+</sup> (Cl <sup>-</sup> ) <sub>2</sub>	B	444.0	Q <sub>x</sub>	587.8 (2.11)	0.0113	H-0 → L+0(+71%)	H-3 → L+1(+25%)
	Q <sub>0</sub>	661.9	Q <sub>y</sub>	582.3 (2.13)	0.0834	H-0 → L+1(+70%)	H-3 → L+0(29%)
H <sub>4</sub> TrPP <sup>2+</sup> (Cl <sup>-</sup> ) <sub>2</sub>	B	436.5	B <sub>x</sub>	367.9 (3.37)	1.3053	H-3 → L+0(+33%)	H-7 → L+1(13%)
	Q <sub>0</sub>	639.9	B <sub>y</sub>	367.0 (3.38)	0.6981	H-3 → L+1(+33%)	H-7 → L+0(+13%)
H <sub>4</sub> DPP <sup>2+</sup> (Cl <sup>-</sup> ) <sub>2</sub>	B	429.0	Q <sub>x</sub>	575.8 (2.15)	0.0050	H-0 → L+0(+56%)	H-3 → L+1(20%)
	Q <sub>0</sub>	622.9	Q <sub>y</sub>	572.7 (2.16)	0.0246	H-0 → L+1(+66%)	H-3 → L+0(+24%)
H <sub>4</sub> P <sup>2+</sup> (Cl <sup>-</sup> ) <sub>2</sub>	B	407.4	B	353.1 (3.51)	0.8310	H-3 → L+1(+15%)	H-3 → L+0(+14%)
	Q <sub>0</sub>	578.9	Q	353.1 (3.51)	0.8310	H-7 → L+0(+9%)	H-7 → L+1(9%)
H <sub>4</sub> TPP <sup>2+</sup> (Cl <sup>-</sup> ) <sub>2</sub>	B	444.0	B	353.1 (3.51)	0.8310	H-3 → L+0(+15%)	H-3 → L+1(14%)
	Q <sub>0</sub>	661.9	Q	566.6 (2.19)	0.0027	H-7 → L+1(9%)	H-7 → L+0(9%)
H <sub>4</sub> TrPP <sup>2+</sup> (Cl <sup>-</sup> ) <sub>2</sub>	B	436.5	B	566.6 (2.19)	0.0024	H-0 → L+0(53%)	H-0 → L+1(+21%)
	Q <sub>0</sub>	639.9	Q	566.6 (2.19)	0.0024	H-3 → L+1(18%)	H-3 → L+0(7%)
H <sub>4</sub> DPP <sup>2+</sup> (Cl <sup>-</sup> ) <sub>2</sub>	B	429.0	B	566.6 (2.19)	0.0024	H-0 → L+1(+53%)	H-0 → L+0(+21%)
	Q <sub>0</sub>	622.9	Q	566.6 (2.19)	0.0024	H-3 → L+0(18%)	H-3 → L+1(+7%)

by comparison of the **ad-porphyrin IV** with parent series (or with **ad-porphyrin II**). From Table 10, we infer that the electronic effect, particularly the electron-donating effect, is the key factor in spectral redshift (both in B and Q bands). The B3LYP calculation results in a similar evaluation.

3.3.3.2. *Porphyrin diacid series*. The TDDFT calculation of several adjusted porphyrin diacid models is also summarized in Tables S40 and S41; the redshift analysis, particularly with regard to the electronic effect of *meso*-phenyl group and the conformational effect is summarized in Table 10.

(1) *Conformational effect*. The redshift induced by the conformational distortion is evaluated by analysis of TDDFT calculations for the **ad-porphyrin I** series (Tables S40 and S41). In PBE1PBE calculations, the predicted total redshift in the **ad-porphyrin I** is

**Table 10**  
Predicted redshift (in nm) with *meso*-phenyl substitution for each effect.

Effect	Redshift (in nm)			
	Zinc porphyrin		Porphyrin diacids	
	B	Q	B	Q
B3LYP method				
Total	30.2	32.8	43.7	22.5
Electron effect	26.8	26.6	30.1	8.7
Donating	19.6	16.2		
Delocalization	7.2	10.4		
Conformational effect	3.4	6.2	11.1	17.7
In-plane	1.0	3.7	1.8	4.5
Out-of-plane	2.4	2.5	11.3	16.9
PBE1PBE method				
Total	30.9	34.1	44.3	48.0
Electron effect	27.3	28.0	30.9	43.1
Donating	19.3	16.1	17.8	12.6
Delocalization	8.0	11.9	13.1	30.5
Conformational effect	3.6	6.1	10.7	16.9
In-plane	0.9	3.2	1.4	3.4
Out-of-plane	2.7	2.9	11.3 (16.9 <sup>a</sup> )	16.8 (24.2 <sup>a</sup> )

<sup>a</sup> With *p*-H<sub>4</sub>P<sup>2+</sup>(Cl<sup>-</sup>)<sub>2</sub> as reference.

10.7 nm for the B band and 16.9 nm for the Q band, respectively. Further, the conformational effect could be divided into in-plane and out-of-plane distortion effects.

The contribution of in-plane distortion could be evaluated by comparison of H<sub>4</sub>P<sup>2+</sup>(Cl<sup>-</sup>)<sub>2</sub> derivatives in **ad-porphyrin I** with its further modulated derivative (labeled as *i*-H<sub>4</sub>P<sup>2+</sup>(Cl<sup>-</sup>)<sub>2</sub>), wherein the partial structure surrounding the C<sub>m</sub> atom, including bond length and bond angle, is adjusted to that of the H<sub>4</sub>TPP<sup>2+</sup>(Cl<sup>-</sup>)<sub>2</sub> derivative in **ad-porphyrin I**. The in-plane variation of the pyrrolic ring is negligible and, therefore, is not considered here. The TDDFT calculation on *i*-H<sub>4</sub>P<sup>2+</sup>(Cl<sup>-</sup>)<sub>2</sub> produces a redshift of approximately 1.4 (B band) and 3.4 nm (Q band) with regard to the H<sub>4</sub>P<sup>2+</sup>(Cl<sup>-</sup>)<sub>2</sub> derivative in **ad-porphyrin I** (Table 10 and Table S40).

The redshift generated by the out-of-plane distortion could be deduced by comparison of H<sub>4</sub>P<sup>2+</sup>(Cl<sup>-</sup>)<sub>2</sub> derivatives in **ad-porphyrin I** with its other further-adjusted derivative (labeled as *o*-H<sub>4</sub>P<sup>2+</sup>(Cl<sup>-</sup>)<sub>2</sub>), wherein the nonplanar degree (denoted by C<sub>α</sub>C<sub>m</sub>C<sub>α</sub>N dihedral angle) is adjusted to that of the H<sub>4</sub>TPP<sup>2+</sup>(Cl<sup>-</sup>)<sub>2</sub> derivative in **ad-porphyrin I**. Calculation on the *o*-H<sub>4</sub>P<sup>2+</sup>(Cl<sup>-</sup>)<sub>2</sub> provides the 11.3 (B band) and 16.8 nm (Q band) redshift (Table 10 and Table S40). The sum of the redshift deduced from *i*-H<sub>4</sub>P<sup>2+</sup>(Cl<sup>-</sup>)<sub>2</sub> and *o*-H<sub>4</sub>P<sup>2+</sup>(Cl<sup>-</sup>)<sub>2</sub> is a slightly greater than that observed from **ad-porphyrin I**; this indicates that in-plane and out-of-plane distortion, in general, become admixed to a certain extent. From the above analysis, we conclude that the conformational effect is generated primarily by out-of-plane distortion for porphyrin diacids.

Fig. 6 depicts the variation of spectral redshift induced by conformational distortion with the extent of *meso*-phenyl substitution as predicted by the PBE1PBE and B3LYP methods; the calculated data are fitted by a polynomial function. From Fig. 6, it is evident that the PBE1PBE and B3LYP calculations have nearly conforming predictions with regard to the conformational effect for both zinc complexes and diacid derivatives. In general, conformational distortion produces a profile with a positive and increasing slope for both B and Q bands; this is similar to the performance of out-of-plane distortions observed in the published literature [9]. The profile of porphyrin diacid series has a larger slope than that of

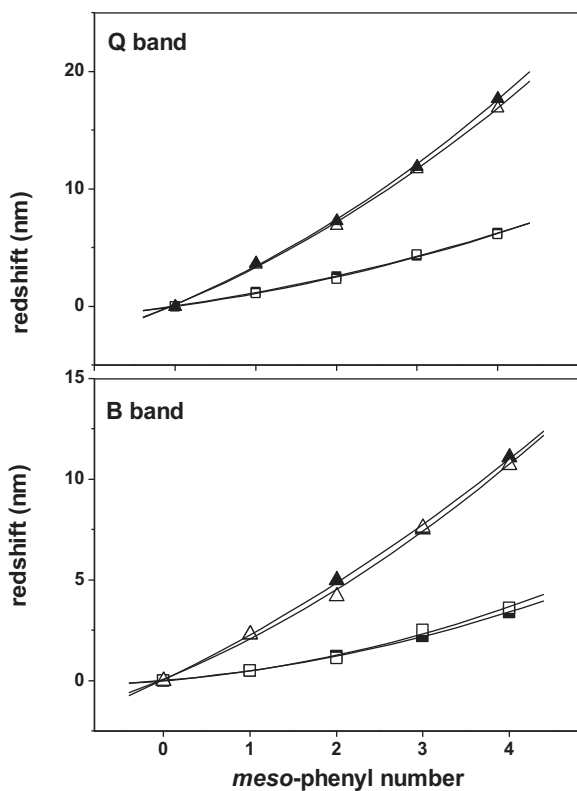


**Fig. 6.** Predicted dependence of redshift caused by conformational effect on *meso*-phenyl number for zinc porphyrin (quadrangle) and porphyrin diacids (triangle). The open data are predicted by PBE1PBE method and solid data are predicted by B3LYP method.

zinc porphyrins; this is attributed to the larger out-of-plane distortion in the former series as compared with the latter series. Therefore, the conformational effect can be inferred to contribute more significantly to spectral redshift in diacids series than in the zinc complexes series.

The  $H_4P^{2+}(Cl^-)_2$  has undergone significant out-of-plane distortion; therefore, application of  $H_4P^{2+}(Cl^-)_2$  derivatives in the **ad-porphyrin I** series as the reference would underestimate the redshift induced by out-of-plane distortion. The selection of a planar porphyrin model as the reference would generate a more credible evaluation. Table S40 presents the TDDFT calculation (in PBE1PBE method) of a planar derivative of  $H_4P^{2+}(Cl^-)_2$  in the **ad-porphyrin I** (labeled as *p*- $H_4P^{2+}(Cl^-)_2$ ), wherein the pyrrolic ring is adjusted to be coplanar with the mean plane of the porphyrin ring. Employing this as a planar model for reference ascribes an additional 5.6 (B band) and 7.4 nm (Q band) redshift to out-of-plane distortions.

(2) *Electronic effect of meso-phenyl group.* The comparison of TDDFT calculations of parent porphyrin diacids with that of **ad-porphyrin II** series (Tables S40 and S41) can generate an estimation of the redshift induced by the electronic effect of the *meso*-phenyl group. The shift distance predicted by the PBE1PBE method, 30.9 nm (B band) and 43.1 nm (Q band), for porphyrin diacids is greater than that of zinc porphyrin; this is attributed to the probable enhanced interaction between the porphyrin and phenyl rings caused by intensified out-of-plane distortion. In addition, we attempted to evaluate the electronic effect by comparing **ad-porphyrin III** and I series. However, the calculation generated a more complicated B band for the **ad-porphyrin III** series (see the result of  $H_4DPP^{2+}(Cl)_2$  listed in Table S42, for example); therefore, this confounds the evaluation, and proves again that the theoretical

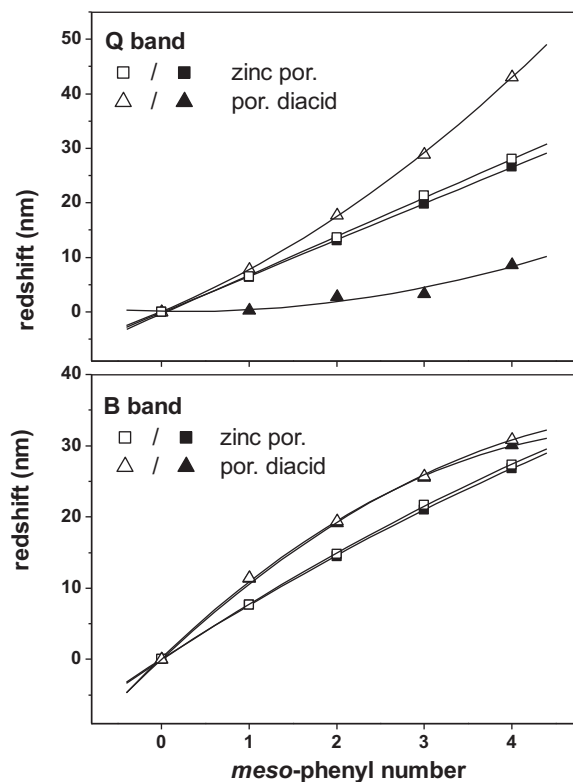


**Fig. 7.** Predicted dependence of redshift caused by electronic effect of *meso*-phenyl group on *meso*-phenyl number for zinc porphyrin (quadrangle) and porphyrin diacids (triangle). The open data are predicted by PBE1PBE method and solid data are predicted by B3LYP method.

simulation of absorption spectra should consider the influence of the counterion.

The electronic effect of the *meso*-phenyl group predicted by the PBE1PBE method generates a profile with a positive but decreasing slope for the B band (Fig. 7). The B3LYP method provides a similar prediction. It is apparent that the profile of zinc porphyrins approaches that of the porphyrin diacids series, and the slight discrepancy observed can be attributed to differences in the extent of the  $\pi$ -electron delocalization effect.

The PBE1PBE and B3LYP methods have similar predictions for the Q band of zinc porphyrins. However, this is not applicable for the Q band of porphyrin diacids; the profile predicted by the PBE1PBE method has a much larger slope than that predicted by the B3LYP method, which indicates that the simulation of the Q band of porphyrin diacids is quite sensitive to the calculation method applied.

Further differentiation of the  $\pi$ -electron delocalization effect from the electron-donating effect can be performed by comparison of **ad-porphyrin IV** with the parent porphyrin or with **ad-porphyrin II**. The TDDFT calculation of **ad-porphyrin IV** by the PBE1PBE method (Table S40) demonstrates that the Q band is more sensitive to the orientation of the *meso*-phenyl group than B band; therefore, it is significantly redshifted under the influence of the  $\pi$ -electron delocalization effect. Nonetheless, the differentiation of the delocalization and electron-donating effects by B3LYP calculation has failed due to the smaller absorption wavelength of the Q band predicted in the **ad-porphyrin IV** series in comparison with the **ad-porphyrin II** series (Table S41); this generates a negative value for the electron-donating effect of the *meso*-phenyl group. This indicates that the B3LYP method is less credible in the evaluation of a weakly interacting system.

(3) *Electronic effect of counterion.* The comparison of the **ad-porphyrin I** series with II series of the diacid species reveals the

effect of the counterion  $\text{Cl}^-$ . Both PBE1PBE and B3LYP methods predict a greater redshifted B band and a less redshifted Q band for the **ad-porphyrin II** series than for the **ad-porphyrin I** series (Tables S40 and S41). The less red-shifted Q band can be attributed to reduced interaction between the porphyrin ring and the  $\text{Cl}^-$  with the extent of *meso*-phenyl substitution.

#### 4. Conclusion

In this study, we employed theoretical calculations to compare structural and spectral variations with the extent of *meso*-phenyl substitution between porphyrin diacids and zinc porphyrins. The PBE1PBE method generates more acceptable results in the TDDFT calculation of porphyrin diacids than the B3LYP and PBEPBE methods. The TDDFT calculation indicates that both out-of-plane distortion and *meso*-phenyl substitution intensify spectral redshift. The influence of the counterion  $\text{Cl}^-$  is complicated. On one hand, the introduction of the  $\text{Cl}^-$  would reduce the HOMO–LUMO gap because of the electron-donating effect of the  $\text{Cl}^-$  ion, which then brings about an additional spectral redshift with regard to the calculation without consideration of counterion. On the other hand, the interaction between the  $\text{Cl}^-$  ion and the porphyrin ring is weakened by *meso*-phenyl substitution; this reduces the redshift size of the Q absorption. The PBE1PBE calculation indicates that the electron-donating effect is the key factor in the redshift of B and Q bands of zinc porphyrin series as well as in the redshift of the B band of porphyrin diacid series; however, the  $\pi$  electron delocalization effect is predicted to be the primary cause of the redshift of Q band of porphyrin diacids series. Meanwhile, out-of-plane distortion is predicted to provide a moderate contribution to the spectral redshift of porphyrin diacids series, because of intensified out-of-plane distortion.

#### Acknowledgment

We thank Professor Shelnutz for kindly helping in NSD calculation and interpretation.

#### Appendix A. Supplementary data

Supplementary data associated with this article can be found, in the online version, at doi:10.1016/j.saa.2011.04.085.

#### References

- [1] M.O. Senge, in: K.M. Kadish, K.M. Smith, R. Guilard (Eds.), *The Porphyrin Handbook*, vol. 1, Academic Press, Boston, 2000, p. 239.
- [2] J.A. Shelnutz, C.J. Medforth, M.D. Berber, K.M. Barkigia, K.M. Smith, *J. Am. Chem. Soc.* 113 (1991) 4077.
- [3] L.D. Spaulding, C.C. Chang, N.-T. Yu, R.H. Felton, *J. Am. Chem. Soc.* 97 (1975) 2517.
- [4] C.-Y. Lin, Y.-C. Wang, S.-J. Hsu, C.-F. Lo, E.W.-G. Diau, *J. Phys. Chem. C* 114 (2010) 687.
- [5] Q. Huang, C.J. Medforth, R. Schweitzer-Stenner, *J. Phys. Chem. A* 109 (2005) 10493.
- [6] A.G. DiMagno, A.K. Wertsching, C.R. Ross, *J. Am. Chem. Soc.* 117 (1995) 8279.
- [7] A.K. Wertsching, A.S. Koch, A.G. DiMagno, *J. Am. Chem. Soc.* 123 (2001) 3932.
- [8] H. Ryeng, A. Ghosh, *J. Am. Chem. Soc.* 124 (2002) 8099.
- [9] R.E. Haddad, S. Gazeau, J. Pecaut, J.-C. Marchon, C.J. Medforth, J.A. Shelnutz, *J. Am. Chem. Soc.* 125 (2003) 1253.
- [10] Z. Zhou, C. Cao, Q. Liu, R. Jiang, *Org. Lett.* 12 (2010) 1780.
- [11] V.N. Knyuksho, K.N. Solovoyov, G.D. Egorova, *Biospectroscopy* 4 (1998) 121.
- [12] Y.-P. Ma, S.-G. He, X.-L. Ding, Z.-C. Wang, W. Xue, Q. Shi, *Phys. Chem. Chem. Phys.* 11 (2009) 2543.
- [13] T. Honda, T. Kojima, S. Fukuzumi, *Chem. Commun.* (2009) 4994.
- [14] G.D. Luca, A. Romeo, L.M. Scolaro, G. Ricciardi, A. Rosa, *Inorg. Chem.* 46 (2007) 5979.
- [15] T. Nakanishi, K. Ohkubo, T. Kojima, S. Fukuzumi, *J. Am. Chem. Soc.* 131 (2009) 577.
- [16] V.S. Chirvony, A. Hoek, V.A. Galievsky, I.V. Sazanovich, T.J. Schaafsma, D. Holten, *J. Phys. Chem. B* 104 (2000) 9909.
- [17] I.V. Avilov, A.Yu. Pannarin, V.S. Chirvony, *Chem. Phys. Lett.* 389 (2004) 352.
- [18] S. Juillard, Y. Ferrand, G. Simonneaux, L. Toupet, *Tetrahedron* 61 (2005) 3489.
- [19] A. Rosa, G. Ricciardi, E.J. Baerends, A. Romeo, L.M. Scolaro, *J. Phys. Chem. A* 107 (2003) 11468.
- [20] Y.-H. Zhang, W.-J. Ruan, Z.-Y. Li, Y. Wu, J.-Y. Zheng, *Chem. Phys.* 315 (2005) 201.
- [21] A.D. Becke, *J. Chem. Phys.* 98 (1993) 5648.
- [22] C. Lee, W. Yang, R.G. Parr, *Phys. Rev. B* 37 (1988) 785.
- [23] J.P. Perdew, K. Burke, M. Ernzerhof, *Phys. Rev. Lett.* 78 (1997) 1396.
- [24] R. Ma, P. Guo, H. Cui, X. Zhang, M.K. Nazeeruddin, M. Gratzel, *J. Phys. Chem. A* 113 (2009) 10119.
- [25] J.P. Perdew, K. Burke, M. Ernzerhof, *Phys. Rev. Lett.* 77 (1996) 3865.
- [26] M.J. Frisch, G.W. Trucks, H.B. Schlegel, G.E. Scuseria, M.A. Robb, J.R. Cheeseman, J.A. Montgomery Jr., T. Vreven, K.N. Kudin, J.C. Burant, J.M. Millam, S.S. Iyengar, J. Tomasi, V. Barone, B. Mennucci, M. Cossi, G. Scalmani, N. Rega, G.A. Petersson, H. Nakatsuji, M. Hada, M. Ehara, K. Toyota, R. Fukuda, J. Hasegawa, M. Ishida, T. Nakajima, Y. Honda, O. Kitao, H. Nakai, M. Klene, X. Li, J.E. Knox, H.P. Hratchian, J.B. Cross, C. Adamo, J. Jaramillo, R. Gomperts, R.E. Stratmann, O. Yazyev, A.J. Austin, R. Cammi, C. Pomelli, J.W. Ochterski, P.Y. Ayala, K. Morokuma, G.A. Voth, P. Salvador, J.J. Dannenberg, V.G. Zakrzewski, S. Dapprich, A.D. Daniels, M.C. Strain, O. Farkas, D.K. Malick, A.D. Rabuck, K. Raghavachari, J.B. Foresman, J.V. Ortiz, Q. Cui, A.G. Baboul, S. Clifford, J. Cioslowski, B.B. Stefanov, G. Liu, A. Liashenko, P. Piskorz, I. Komaromi, R.L. Martin, D.J. Fox, T. Keith, M.A. Al-Laham, C.Y. Peng, A. Nanayakkara, M. Challacombe, P.M.W. Gill, B. Johnson, W. Chen, M.W. Wong, C. Gonzalez, J.A. Pople, *Gaussian Suite Gaussian 03, Revision C.01*, Gaussian, Inc., Wallingford, CT, 2004.
- [27] (a) S.I. Gorelsky, SWizard Program, University of Ottawa, Ottawa, Canada, 2010, <http://www.sg-chem.net/>;  
(b) S.I. Gorelsky, A.B.P. Lever, *J. Organomet. Chem.* 635 (2001) 187.
- [28] D.-M. Chen, X. Liu, T.-J. He, F.-C. Liu, *Chem. Phys.* 289 (2003) 397.
- [29] NSD calculation was carried out online at <http://jasheln.unm.edu/jasheln/content/nsd/NSDengine/start.htm>.
- [30] Y.-H. Zhang, W. Zhao, P. Jiang, L.-J. Zhang, T. Zhang, J. Wang, *Spectrochim. Acta A* 75 (2010) 880.
- [31] W.R. Scheidt, J.U. Mondal, C.W. Eigenbrot, A. Adler, L.J. Radonovich, J.L. Hoard, *Inorg. Chem.* 25 (1986) 795.
- [32] K.A. Nguyen, P.N. Day, R. Pachter, *J. Phys. Chem. A* 103 (1999) 9378.
- [33] B. Cheng, O.Q. Munro, H.M. Marques, W.R. Scheidt, *J. Am. Chem. Soc.* 119 (1997) 10732.
- [34] PBE1PBE calculation on  $(\text{Cl}^-)_2$  cluster that has similar structure with the counterpart in  $\text{H}_4\text{TPP}^{2+}(\text{Cl}^-)_2$  indicates that the *p* orbit of  $(\text{Cl}^-)_2$  involved in G-HOMO orbit has much higher level.